Proc. Natl. Acad. Sci. USA
Vol. 89, pp. 8403–8407, September 1992
Immunology

Crystal structure of the major histocompatibility complex class I H-2K^b molecule containing a single viral peptide: Implications for peptide binding and T-cell receptor recognition

(H-2K^b complex/protein crystallography/T-cell recognition)

WEIGUO ZHANG*, AIDEEN C. M. YOUNG†, MONICA IMARAI*, STANLEY G. NATHENSON*, AND JAMES C. SACCHETTINI†

*Department of Microbiology and Immunology and Department of Cell Biology; and †Department of Biochemistry, Albert Einstein College of Medicine, Bronx, NY 10461

Contributed by Stanley G. Nathenson, June 10, 1992

ABSTRACT **To study the structure of a homogenous major histocompatibility complex (MHC) class I molecule containing a single bound peptide, a complex of recombinant mouse H-2K^b, β_2-microglobulin (β_2m), and a fragment of the vesicular stomatitis virus (VSV) nuclear capsid protein, VSV-(N52–59) octapeptide (Arg-Gly-Tyr-Val-Tyr-Gln-Gly-Leu), was prepared by exploiting a high-yield bacterial expression system and *in vitro* cocomplex formation. The structure of mouse H-2K^b revealed its similarity to three human class I HLA molecules, consistent with the high primary sequence homology and common function of these peptide-presenting molecules. Electron density was located in the peptide-binding groove, to which a single peptide in a unique conformation was unambiguously fit. The peptide extends the length of the groove, parallel to the α-helices, and assumes an extended, mostly β-strand conformation. The peptide is constrained within the groove by hydrogen bonding of its main-chain atoms and by contacts of its side chains with the H-2K^b molecule. The amino-terminal nitrogen atom of the peptide forms a hydrogen bond with the hydroxyl group of Tyr-171 of H-2K^b at one end of the groove, while the carboxyl-terminal oxygen forms a hydrogen bond with the hydroxyl group of Tyr-84 at the other end. Since the amino acids at both ends are conserved among human and mouse MHC molecules, this anchoring of each end of the peptide appears to be a general feature of peptide–MHC class I molecule binding and imposes restrictions on its length. The side chains of residues Tyr-3, Tyr-5, and Leu-8 of the VSV octapeptide fit into the interior of the H-2K^b molecule with no appreciable surface exposure, a finding in support of previous biological studies that showed the importance of these residues for binding. Thus, the basis for binding of specific peptide sequences to the MHC class I molecule is the steric restriction imposed on the peptide side chains by the architecture of the floor and sides of the groove. The side chains of Arg-1, Val-4, and Gln-6 and the main-chain of Gly-7 of the octapeptide are exposed on the surface of the complex, thus confirming their availability for T-cell receptor contact, as previously demonstrated by T-cell recognition experiments.**

Short peptide fragments of intracellularly processed proteins are displayed by major histocompatibility complex (MHC) class I molecules on the cell surface, where the peptide–MHC class I complex is recognized by the T-cell receptors (TCRs) of cytotoxic T lymphocytes (CTLs) (1–5). The MHC class I molecule consists of an α chain of about 350 amino acids noncovalently associated with a β chain [β_2-microglobulin (β_2m)] of 99 amino acids (6). Crystallographic studies with human class I molecules have shown that a potential peptide presentation site exists in the form of a groove located in the most-membrane-distal portion of the MHC class I molecule. The groove is composed of two α-helical regions, which form its sides, and eight antiparallel β-strands, which form its floor (7, 8). Studies of H-2K^b molecules with point mutations suggest that for target recognition to occur, the TCR must interface simultaneously with the α_1- and α_2-helices of the antigen-presentation domain of the MHC class I molecule on the target cell (9), thereby positioning it to contact the amino acid side chains of a peptide bound in the groove.

Much of the diversity among the alleles of the MHC class I molecules, generated by microgene conversion (10), is found in amino acid residues that line the peptide-binding groove (8). This sequence diversity alters the chemical composition and spatial properties of the peptide-binding groove, which in turn dictate the characteristics of those peptides that can be accommodated. For example, in our previous studies, we found that the characteristic motifs of peptides bound to the mouse *H-2K^b* allelic product differ from those of peptides bound to the paralogous H-2D^b molecule or to H-2K^{bm1} and H-2K^{bm8} molecules (3).

In an initial step in the characterization of those peptides that bind to specific MHC class I molecules *in vivo*, we identified the major H-2K^b-restricted peptide from vesicular stomatitis virus (VSV)-infected cells (2) as a unique octamer—namely, VSV-(N52–59), Arg-Gly-Tyr-Val-Tyr-Gln-Gly-Leu. These residues will be identified by their position in the octapeptide and boldface type. Alanine-substituted peptide variants were then used to further define the role of each amino acid residue in the octapeptide in terms of its interaction with the H-2K^b molecule and with the TCR. As a result of these studies, we postulated that **Tyr-3, Tyr-5,** and **Leu-8** are MHC anchor residues, while **Arg-1, Val-4, Gln-6,** and **Gly-7** are important in TCR recognition (11).

To evaluate these hypotheses at the structural level, a peptide–H-2K^b complex was prepared by exploiting bacterial expression and protein-folding techniques to obtain a complex containing a single peptide. The complex was subsequently crystallized for x-ray analysis. The goal of this study was to refine the H-2K^b structure to the point at which the peptide could be unambiguously positioned in the electron density located in the peptide-binding groove. Analysis of the three-dimensional structure of this complex provides precise details of peptide–MHC class I interactions, significantly refining our understanding of the basis for allele-specific peptide-binding motifs and TCR recognition.‡

The publication costs of this article were defrayed in part by page charge payment. This article must therefore be hereby marked "*advertisement*" in accordance with 18 U.S.C. §1734 solely to indicate this fact.

Abbreviations: MHC, major histocompatibility complex; TCR, T-cell receptor; CTL, cytotoxic T lymphocyte; VSV, vesicular stomatitis virus; rms, root-mean-square; β_2m, β_2-microglobulin.

‡The atomic coordinates have been deposited in the Protein Data Bank, Chemistry Department, Brookhaven National Laboratory, Upton, NY 11973 (reference 1MHA).

MATERIALS AND METHODS

Cloning of Genes for H-2K^b and β_2m into a Bacterial Expression Vector. To construct the expression vector of H-2K^b and β_2m, the regions encoding amino acids 1–280 of H-2K^b and amino acids 1–99 of β_2m were amplified by PCR and cloned into pET-3a (12). The expression plasmids were transformed into BL21(DE3)pLysS (Novagen).

Production of Recombinant H-2K^b and β_2m Inclusion Bodies. Transformed BL21(DE3)pLysS cells were grown in Luria-Bertani (LB) medium containing 50 μg of carbenicillin and 10 μg of chloramphenicol per ml. When the culture reached an OD_{600} of 0.6–1.0, isopropyl β-D-thiogalactopyranoside (Sigma) was added to a final concentration of 0.5 mM. The bacteria were harvested ($OD_{600} \approx 1.8$) and lysed with a French press. After centrifugation at 10,000 $\times$ g, the pellet was washed with the lysis buffer (20 mM Tris chloride/23% sucrose/1 mM EDTA) containing 0.5% Triton X-100. Inclusion bodies were about 90% of the pellet.

Preparation of the "H-2K^b Complex" (H-2K^b α Chain–β_2m–Peptide). The inclusion bodies of H-2K^b and β_2m were dissolved in 20 mM Tris chloride, pH 8.0/4 M urea. Nine milligrams of H-2K^b was mixed with 3 mg of β_2m and 2 mg of VSV-(N52–59) peptide; the mixture was dialyzed against 20 mM Tris·HCl/150 mM NaCl, pH 8.0, at 4°C in Spectra/Por CE dialysis tubing (Spectra, MWCO 500) for 24 hr. After dialysis the soluble portion was concentrated and then chromatographed on a Syperdex G-75 column (Pharmacia) equilibrated with 20 mM Tris·HCl/150 mM NaCl, pH 8.0. The H-2K^b complex was eluted as a single peak corresponding to a protein of about 45 kDa. Further purification of the complex was carried out on Mono Q column (Pharmacia) with a gradient of 0–0.60 M NaCl.

Crystallization of the H-2K^b Class I Complex. The conditions for crystallization of the H-2K^b complex were established by the sparse-scan technique (13) with the "hanging drop" vapor-diffusion method. The best crystals in the sparse scan were obtained when 0.2 M magnesium acetate/0.1 M cacodylate buffer, pH 6.5/12–15% polyethylene glycol 8000 was used as the reservoir buffer.

Data Collecting and Processing. X-ray diffraction data were collected on a Siemens area detector system coupled to a Rigaku RU-200 rotating anode x-ray generator. Diffraction data to 2.8-Å resolution were collected from one crystal of the H-2K^b complex (19,176 unique reflections, 79.5% complete at 2.8 Å). The mean intensity I/σ was 3.34 with a mean observation-to-reflection ratio of 1.91. The symmetry-derived R factor based on intensity for the entire data set was 14.6%. Pseudo-precession photographs of the diffraction data were used to determine that the space group symmetry was $P2_1$. The unit-cell parameters were a = 90.9 Å, b = 92.2 Å, c = 67.5 Å, and β = 111.24°.

Structure Solution. The tertiary structure of H-2K^b was solved by using the molecular replacement option of the X-PLOR program package (14) with the refined structure of HLA-A2 (7) as a starting model. The rotation function was first solved with data from 15.0 Å to 4.0 Å and gave a single solution at α = 35.0°, β = 90.0°, and γ = 267.5°. A subsequent translation search yielded two solutions, corresponding to the two molecules of the asymmetric unit. A combined translation search located the relative translation of the second molecule to the first. Rigid body refinement with X-PLOR was then carried out on the orientations of both molecules and gave an R factor of 37.7%.

Refinement of the H-2K^b Complex to 2.8-Å Resolution. Energy refinement, simulated annealing (14) least-squares refinement (TNT program; ref. 15), and model building were used to improve the structure of the H-2K^b complex at 2.8-Å resolution. The first cycle of refinement employed simulated annealing with X-PLOR. This model contained no bound peptide or solvent molecules and retained the primary sequence of HLA-A2. The structure was slow-cooled from 3000 K to 300 K in steps of 25 K as described in the X-PLOR manual.

The H-2K^b–β_2m molecule was then assigned its correct amino acid sequence by replacing residues with the molecular model-building software TOM. Only the first 270 amino acids of the α polypeptide were assigned because of disorder of the C-terminal tail. Difference electron density in the peptide-binding groove of both molecules, as observed on a $|F_{obs}| - |F_{calc}|$ electron-density map, was modeled as eight residues of alanine. The structure was further refined as described above, leading to a R factor of 21.9%. The VSV-(N52–59) peptide in each H-2K^b molecule was then built. Manual adjustment of some residues of the protein was followed by energy refinement of the positions and temperature factors of each atom, leading to a R factor of 21.8%. Refinement of the model was completed by using conventional least-squares refinement with TNT (15). The geometric restraints were first relaxed during five cycles of refinement and then gradually increased during 10 subsequent cycles until the final root-mean-square (rms) bond length, bond angle, and torsion angle deviations were 0.019 Å^2, 2.94°, and 22.5°, respectively. Refinement of the individual atomic temperature factors led to a final R factor of 18.4%.

RESULTS

Overall Description of the H-2K^b Complex. We have found no major differences between two H-2K^b complex molecules in the asymmetric unit. Therefore, we limit the description of the H-2K^b molecule to an averaged structure. (The rms difference between the main-chain atoms of the heavy chains of the two molecules in one asymmetric unit is 0.93 Å and 0.81 Å for the two light chains.) The 2.8-Å resolution structure of the H-2K^b complex contains 6160 protein atoms. No ordered buffer atoms, ions, or ordered water molecules were placed in the electron density maps. The final R factor of the refined model was 18.4%, indicating good agreement between the observed data and the calculated model. The final structure showed good agreement with canonical stereochemistry, as demonstrated by its rms deviations from standard geometry of 0.019 Å^2 for bond distances, 2.90° for bond angles, and 22.5° for torsional angles. The mean temperature factors (indicating the degree to which an atom is vibrating about its mean position) for main-chain and side-chain atoms of the heavy chain were 19.9 Å^2 and 21.1 Å^2, respectively. Although the corresponding values for β_2m were lower, at 13.7 Å^2 and 18.9 Å^2, respectively, both chains showed temperature factors in the range expected for a well-ordered crystalline protein.

The structure of the H-2K^b complex contains the first 270 residues of the α polypeptide, β_2m, and a bound octapeptide (Fig. 1). H-2K^b is similar to human HLA-A2 (7, 16–18). In fact, the rms difference between the main-chain atoms of the α chains of the two structures is 1.9 Å^2 and that between the corresponding β_2m chains is 0.8 Å^2, indicating that the overall structure of recombinant mouse H-2K^b molecule is essentially identical to that of the human lymphocyte-derived MHC class I HLA-A2 molecule. Such structural similarities are consistent with the common function and high sequence homology between mouse and human class I molecules. A description of the overall structure of the MHC class I molecule has been previously provided by Bjorkman et al. (7).

Conformation of the Peptide. The bound octapeptide resides in the cleft of the peptide recognition domain in a single and well-ordered conformation. Clearly defined electron density in the binding groove permitted the placement of each atom of the eight residues of the bound peptide (Fig. 2). The Φ and Ψ angles for the bound octapeptide indicate that all

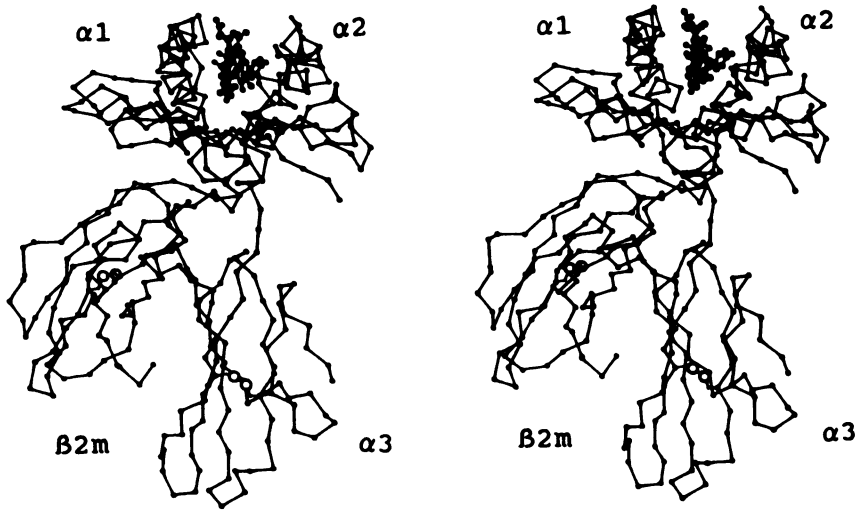

FIG. 1. Stereoview of the α-carbon model of H-2K^b showing the α and β chains and the bound VSV-(N52–59) octapeptide between the α_1- and α_2-helices. In this orientation the peptide-binding groove is being viewed down its length from the **Arg-1** end of the peptide.

residues, with the exception of **Gly-7**, are in a β-strand conformation (data not shown). At 79° and 161° respectively, the Φ and Ψ angles for **Gly-7** occur in a region of the Ramachandran plot that is only permissible for glycine residues because of their lack of a side chain. These Φ and Ψ angles would be sterically prohibited for all other residues. Distinct electron density for **Arg-1**, **Val-4**, and **Gln-6** shows that these residues are directed out of the binding cleft, while **Tyr-5** and **Leu-8** reside deep in its interior. **Tyr-3** is directed up under the lip of the α_2-helix (Figs. 3 and 4).

The solvent accessible surface area of all the atoms and of the main-chain atoms of each octapeptide residue has been calculated by using the Connolly algorithm (19). **Arg-1**, **Val-4**, and **Gln-6** are oriented toward the exterior (Fig. 3) and have the largest solvent-accessible surface areas (39 Å^2, 77 Å^2, and 103 Å^2, respectively). The side chains of **Tyr-3**, **Tyr-5**, and **Leu-8** are in the interior of the cleft, and their solvent-accessible surface areas are correspondingly low (11 Å^2, 4 Å^2 and 7 Å^2, respectively). In particular, **Tyr-5** has the lowest side-chain accessibility, and the structure reveals that it is located deeper in the groove than any other residue of the octamer (Figs. 3 and 4). The solvent-accessible surface area that has been calculated by using main-chain atoms only permits a comparison of the two glycine residues of the peptide and indicates that the main-chain atoms of **Gly-7** have an appreciable solvent-accessible surface area (14 Å^2), particularly when compared with **Gly-2** (3 Å^2).

Interactions of the Peptide with the Groove. A number of electrostatic interactions appear to be critical for the binding of the octapeptide to the groove (Fig. 2). All of the hydrogen bonds formed between the peptide and the residues of the groove involve the main-chain atoms of the peptide. The N-terminal amino group of the peptide is oriented towards the interior of the groove, where it forms a hydrogen bond with the hydroxyl group of Tyr-171 of H-2K^b. The carbonyl oxygen of **Arg-1** is directed towards the floor of the groove and forms a hydrogen bond with the hydroxyl group of Tyr-159. The main-chain nitrogen of **Gly-2** forms hydrogen bonds with both side-chain oxygen atoms of Glu-63, while its carbonyl oxygen forms hydrogen bonds with N$^\varepsilon$ of Lys-66. This latter residue appears to straddle the groove. The carbonyl oxygen of **Tyr-3** points at the interior of the wall of the groove below the α_2-helix and forms hydrogen bonds with N$^{\delta 2}$ of Asn-70, which is directed into the interior of the groove. A hydrogen bond exists between the main-chain nitrogen atom of **Tyr-5** and the side-chain oxygen of Asn-70. The nitrogen atom of the indole ring of Trp-147 forms a hydrogen bond with the carbonyl oxygen of **Gln-6**. The carbonyl oxygen atom of **Gly-7** is involved in hydrogen bonding interactions with both side-chain oxygen atoms of Asp-77. At the C-terminal end of the peptide, one of the terminal oxygen atoms of **Leu-8** hydrogen bonds with the hydroxyl group of Tyr-84. It is located under Lys-146 which protrudes out over the top of the groove.

The side chains of **Tyr-3** and **Tyr-5** form no hydrogen bonds with atoms of the protein. Both tyrosine residues are located in spacious depressions, forming van der Waals contacts with aromatic and hydrophobic residues of the binding groove. The side chain of **Leu-8** is stabilized by van der Waals contacts with residues Tyr-116 and Tyr-123 pointing up from the floor of the binding cleft and with other residues lining both walls of the groove.

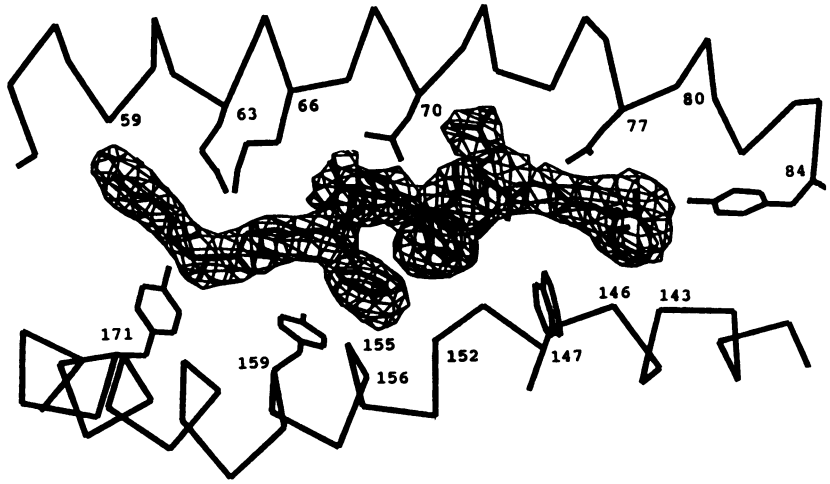

FIG. 2. Diagram of the α-carbon backbone of the α_1- and α_2-helices of H-2K^b and the bound VSV-(N52–59) octapeptide model superimposed on 2.8-Å difference electron density in the antigen-binding groove between the helices. In this orientation the peptide-presentation domain is viewed from above with **Arg-1** on the left and **Leu-8** on the right. The side chains of those residues involved in hydrogen bonding with main-chain atoms of the peptide are shown, and other residues that are potential hydrogen bond donors or acceptors are also indicated.

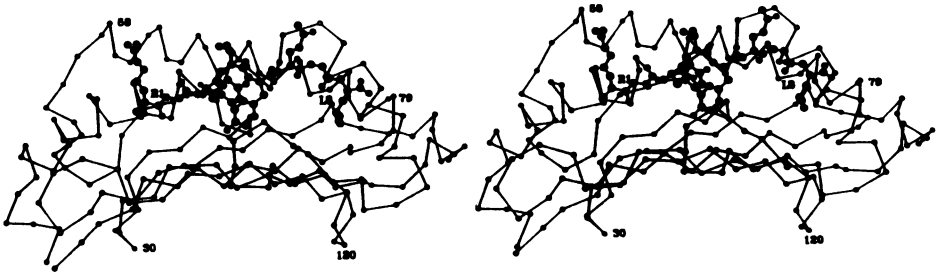

FIG. 3. Stereodiagram of the α-carbon backbone of the α_1- and α_2-helices of H-2K^b with the bound VSV-(N52–59) peptide. In this representation the peptide-binding groove is viewed from the side so that the α_2-helix is in the foreground and the α_1 helix is behind the peptide.

DISCUSSION

The present studies are part of our approach to define the rules for peptide binding to MHC class I molecules and for the recognition of the complex by the TCR. Analysis of the structure of the H-2K^b complex and correlation with biological studies reveals three levels of protein–protein interaction that appear to be critical to antigen presentation and TCR recognition.

(*i*) Hydrogen bonds between main-chain atoms of the peptide and residues of the groove impose restrictions on the length of the peptide that can bind to MHC class I molecules.

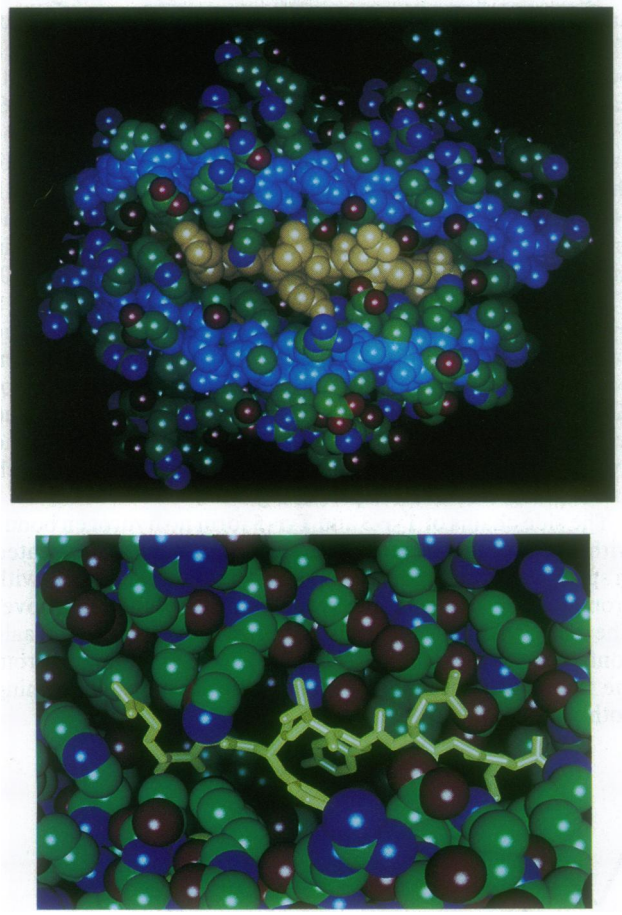

FIG. 4. (*Upper*) CPK representation of the H-2K^b–peptide complex, illustrating the structural complementarity between the octapeptide and the H-2K^b binding groove. The peptide presentation site is viewed from above with the peptide shown in light green. **Arg-1** is on the left and **Leu-8** on the right of the binding groove. Carbon atoms are shown in green, oxygen atoms in red, and nitrogen atoms in dark blue. The main-chain atoms of the α_1- and α_2-helices are highlighted in light blue. (*Lower*) Close-up view of the complex where the octapeptide is shown in light green tubes, revealing the spatial properties of the groove; **Arg-1**, **Val-4**, and **Gln-6** are seen to be directed out of the binding groove. Color coding of atoms is as in *Upper*, except that the α-helices are not shown in light blue.

(*ii*) The architecture of the groove imposes restrictions on the nature of those peptide side-chains that can be accommodated. Thus, the structure of the groove, which varies among MHC class I molecules of different alleles, determines the position and identity of the anchor residues in the peptide.

(*iii*) The TCR recognizes a composite structure formed by the MHC molecule–peptide complex and interacts with surface accessible side chains of the peptide.

Hydrogen Bonds Between the Peptide and Amino Acids of Conserved Regions at the Ends of the Groove Determine the Length of the Peptide That Can Bind. The MHC class I H-2K^b molecule binds a single VSV peptide in only one orientation. Main-chain hydrogen bonds along the length of the peptide position it in the groove (Fig. 2). The amino terminus is located at one end of the groove, close to the highly conserved residues Tyr-59, Tyr-171, and Trp-167, and forms a hydrogen bond with the hydroxyl group of Tyr-171. The carboxyl terminus is anchored at the other end of the groove in another conserved region in the interior of the H-2K^b molecule, through a hydrogen bond with the hydroxyl group of Tyr-84 (Fig. 2). These anchor hydrogen bonds involving Tyr-171 and Tyr-84 have also been proposed for a model nonameric peptide in the HLA-B27 cleft (16), suggesting that these interactions are a general feature of peptide binding to class I molecules. This feature of peptide binding would set a limit on the minimum size of the peptide that can bind and is consistent with our previous studies (11), where the truncation of single residues at either the N or C terminus was seen to significantly curtail binding.

The number of residues in peptides that bind to H-2K^b appears to be eight or nine. For example, while VSV (2) and ovalbumin peptides (20) are composed of eight residues, a peptide from Sendai virus (21) was found to be nine residues long. For HLA-A2, a series of peptides with identical eight- or nine-residue cores but varying in length from 9 to 12 amino acids have been shown to bind to this human class I molecule (22, 23). Two possible explanations for the binding of longer peptides to HLA-A2 can be proposed, assuming conservation of main-chain hydrogen bonds involving Tyr-84 and Tyr-171. In the first possibility, these anchor hydrogen bonds are maintained with the termini of the peptide, forcing it into a conformation that would cause it to buckle. This appears to be the case for the modeled nonamer of HLA-B27, where a kink is proposed to occur at amino acids **Tyr-3** and **Val-4** (16). A second possibility for the binding of longer peptides to class I molecules, is that the hydroxyl groups of Tyr-84 and Tyr-171 hydrogen bond to nonterminal main-chain atoms of the peptide, with additional amino acids at either end of the peptide extended out of the groove.

The existence of specific hydrogen bonds between amino acids of the H-2K^b molecule and the bound peptide may be the basis for variations in CTL response in some *H-2K^b* mutant mice. For example, H-2K^{bm3} and H-2K^{bm11}, which have a Asp-77 → Ser change (10), were discovered to be low responders or nonresponders to VSV (24) and Sendai viruses (25). As mentioned before, Asp-77 forms hydrogen bonds to the carbonyl oxygen of **Gly-7** of the VSV peptide. Hence, the Asp-77 → Ser change would interfere with peptide binding.

Allele-Specific Architecture of the Groove Plays a Role in the Selection of the Specific Peptides That Will Be Presented. The three-dimensional structure of the H-2K^b complex at 2.8-Å resolution provides structural proof of our predictions that **Tyr-3, Tyr-5**, and **Leu-8** anchor the peptide in the groove, since their side chains fit into spacious depressions within the MHC molecule and have low solvent accessibility (Fig. 4). The side chains of these three residues are held in place by van der Waals interactions with the side chains of MHC residues that line the groove. Our peptide binding studies (3) and those of Rammensee and co-workers (4) show that there is a strong preference for an aromatic residue (mostly tyrosine and phenylalanine) at positions 3 and 5 and for a bulky hydrophobic residue at position 8. This preference is further illustrated by the studies in which substitutions at any one of these positions by alanine dramatically reduces peptide binding to H-2K^b (11).

We did not find hydrogen bonds formed between the hydroxyl groups of either **Tyr-3** or **Tyr-5** and residues of the groove. It is possible that the hydroxyl groups form hydrogen bonds to bridging water molecules, for which there appear to be ample room in the tyrosine binding sites. Higher resolution data will be required to ascertain the presence of such ordered water molecules.

An alteration in the interactions of the peptide side chains with the residues of the MHC groove is suggested in studies of the H-2K^{bm1} (10) mutant, which is also a nonresponder in its CTL immune response to VSV (24) and Sendai viruses (25). Previous studies showed that there were profound differences in the set of peptides complexed with H-2K^{bm1}, compared with the set bound to native H-2K^b (3). Tyrosine at position 3 was not found in any of the peptides bound to H-2K^{bm1}. The three-dimensional structure of the H-2K^b groove clearly points out a basis for these findings. **Tyr-3** of the VSV-(N52–59) octapeptide is positioned close to the side chains of Glu-152, Arg-155, and Leu-156 (Fig. 2). The H-2K^{bm1} mutant molecule contains bulky tyrosine residues at 155 (for wild-type arginine) and 156 (for wild-type leucine) and alanine at 152 (for wild-type glutamic acid). In particular, the replacement of Arg-155 and Leu-156 by tyrosine would greatly reduce the space available for the side chain of **Tyr-3.**

Therefore, it appears that the lack of response to VSV in the *H-2K^{bm1}* mouse may be due to a lack of VSV peptide binding or to binding in an altered conformation, since in the *H-2K^b* mouse the VSV-(N52–59) peptide appears to be the only dominant epitope observed for the antiviral response. However, it is likely that the nonresponsiveness in *H-2K^{bm1}* mice may also be due to a direct effect on virus-specific TCR interaction with H-2K^b, caused by the Arg-155 → Tyr change, as the latter is located on the lip of the α_2-helix (Fig. 2). Thus, alterations of both TCR recognition and VSV peptide binding may be expected to play a role in the lack of CTL immune response for the H-2K^{bm1} mutant.

TCR Interacts with Amino Acids Positioned Along the Length of the Peptide That Have a High Solvent-Accessible Surface Area. Five of the eight peptide residues of VSV-(N52–59) are potential TCR contact residues because of their orientation in the groove (Figs. 3 and 4). Our previous analysis with five VSV-specific clones tested with peptides in which the residue in question had been substituted by alanine showed that each clone required contact with a subset of residues—namely, **Arg-1, Val-4, Gln-6**, and **Gly-7** (11). These recognition patterns are consistent with the high solvent accessibility of the side chains of **Arg-1, Val-4**, and **Gln-6** and the main-chain atoms of **Gly-7.** Although the relatively high solvent-accessible surface area of **Gly-7** may indicate that some TCRs can contact its main-chain atoms, it is also the case that the replacement of **Gly-7** with alanine would result in a major conformational change of the peptide, since the Φ and Ψ angles of **Gly-7** are sterically not allowed for alanine.

Concluding Remarks. The solution of the structure of the VSV-(N52–59)–H-2K^b complex has significantly improved our understanding of the structural strategy by which the MHC class I molecule functions. Features of peptide binding, including main-chain hydrogen bonds and side-chain interactions with architecturally complementary regions of the groove, form the basis of peptide binding to the peptide-presentation domain. As a consequence of its conformation in the groove, only four amino acid residues of the peptide are available for TCR contact, whereas the side chains of three residues of the peptide anchor it in the groove. Together with the analysis of other peptide MHC structures and refinement of our understanding of the biological processing of protein antigens, these studies will facilitate our ability to prepare peptide vaccines and to understand the features important in autoimmune diseases.

We thank M. Scharff, B. Birshtein, S. Almo, G. M. van Bleek, and S. Joyce for reviewing the manuscript, R. Angeletti for her invaluable suggestions, The Einstein DNA facility for the synthesis of oligonucleotides, the Laboratory of Macromolecular Analysis for the synthesis of peptides, and P. Reiner for color graphics. We also thank B. Arnold and P. Kourilsky for providing us with H-2K^b cDNA and β_2m cDNA and R. Spata for excellent typing. This work was supported by National Institutes of Health Grants 5 R37 AI-07289, 1 RO1 GM45839, 2 PO1 AI-10792, 2 P30 CA 13330, and 1 RO1 AI-27199.

1. Townsend, A. R. M., Gotch, F. M. & Davey, J. (1985) *Cell* **42,** 457–467.
2. Van Bleek, G. M. & Nathenson, S. G. (1990) *Nature (London)* **348,** 248–251.
3. Van Bleek, G. M. & Nathenson, S. G. (1991) *Proc. Natl. Acad. Sci. USA* **88,** 11032–11036.
4. Falk, K., Rotzschke, O., Stevanovic, S., Jung, G. & Rammensee, H. G. (1991) *Nature (London)* **351,** 290–296.
5. Falk, K., Rotzschke, O. & Rammensee, H.-G. (1990) *Nature (London)* **348,** 248–250.
6. Nathenson, S. G., Uehara, H., Ewenstein, B. M., Kindt, T. J. & Coligan, J. E. (1981) *Annu. Rev. Biochem.* **50,** 1025–1052.
7. Bjorkman, P. J., Saper, M. A., Samaraoui, B., Bennett, W. S., Strominger, J. L. & Wiley, D. C. (1987) *Nature (London)* **329,** 506–512.
8. Bjorkman, P. J., Saper, M. A., Samaraoui, B., Bennett, W. S., Strominger, J. L. & Wiley, D. C. (1987) *Nature (London)* **329,** 512–518.
9. Ajitkumar, P., Geier, S. S., Kesari, K. V., Borriello, F., Nakagawa, J. A., Bluestone, M. A., Saper, M. A., Wiley, D. C. & Nathenson, S. G. (1988) *Cell* **54,** 47–56.
10. Nathenson, S. G., Geliebter, J., Pfaffenbach, G. M. & Zeff, R. A. (1986) *Annu. Rev. Immunol.* **4,** 471–502.
11. Shibata, K. I., Imarai, M., Van Bleek, G. M., Joyce, S. & Nathenson, S. G. (1992) *Proc. Natl. Acad. Sci. USA* **89,** 3135–3139.
12. Studier, F. W., Rosenberg, A. H., Dunn, J. J. & Dubendorff, J. W. (1990) *Methods Enzymol.* **195,** 60–89.
13. Jancarik, J. & Kim, S.-H. (1991) *J. Appl. Cryst.* **24,** 409–411.
14. Brünger, A. T., Kuriyan, J. & Karplus, M. (1987) *Science* **223,** 458–460.
15. Tronrud, D. E., TenEyck, L. F. & Matthews, B. W. (1988) *Acta Crystallogr.* **43,** 489–501.
16. Madden, D. R., Gorga, J. C., Strominger, J. L. & Wiley, D. C. (1991) *Nature (London)* **353,** 321–325.
17. Garrett, T. P. J., Saper, M. A., Bjorkman, P. J., Strominger, J. L. & Wiley, D. C. (1989) *Nature (London)* **342,** 692–696.
18. Gorga, J. C., Madden, D. R., Prendergast, J. K., Wiley, D. C. & Strominger, J. L. (1991) *Proteins Struct. Funct. Genet.* **12,** 87–90.
19. Connolly, W. L. (1985) *J. Am. Chem. Soc.* **107,** 1118–1124.
20. Carbone, F. R. & Bevan, M. J. (1989) *J. Exp. Med.* **169,** 603–612.
21. Schumacher, T. N. M., Heemels, M.-T., Neefjes, J., Kast, W. M., Melief, C. J. M. & Ploegh, H. L. (1990) *Cell* **62,** 563–567.
22. Henderson, R. A., Michel, H., Sakaguchi, K., Shabanowitz, J., Appella, E., Hunt, D. F. & Engelhard, V. H. (1992) *Science* **255,** 1264–1266.
23. Wei, M. L. & Cresswell, P. (1992) *Nature (London)* **356,** 443–446.
24. Clark, S. S. & Forman, J. (1983) *Transpl. Proc.* **15,** 2090–2092.
25. de Waal, L. P., Kast, W. M., Melvold, R. W. & Melief, C. J. M. (1983) *J. Immunol.* **130,** 1090–1096.